ADVANCED MATERIALS
www.advmat.de

Synthetic Active Liquid Crystals Powered by Acoustic Waves

Andrey Sokolov, Jaideep Katuri, Juan J. de Pablo, and Alexey Snezhko*

Active nematic materials combine orientational order with activity at the microscopic level. Current experimental realizations of active nematics include vibrating elongated particles, cell layers, suspensions of elongated bacteria, and a mixture of bio-filaments with molecular motors. The majority of active nematics are of biological origin. The realization of a fully synthetic active liquid crystal comprised of a lyotropic chromonic liquid crystal energized by ultrasonic waves, is reported. This synthetic active liquid crystal is free from biological degradation and variability, exhibits phenomenology associated with active nematics, and enables precise and rapid activity control over a significantly extended range. It is demonstrated that the energy of the acoustic field is converted into microscopic extensile stresses disrupting long-range nematic order and giving rise to an undulation instability and proliferation of topological defects. The emergence of unconventional free-standing persistent vortices in the nematic director field at high activity levels is revealed. The results provide a foundation for the design of externally energized active liquid crystals with stable material properties and tunable topological defect dynamics crucial for the realization of reconfigurable microfluidic systems.

1. Introduction

The diverse phenomenology of active nematics arises from a combination of the anisotropic characteristics of the unitary building blocks and their non-equilibrium behavior.[1–9] The hallmark feature of active nematics is a continuous reconfiguration of the orientational order and the spatiotemporal variations of the order parameter, frequently called 'active turbulence', arising from the interplay between anisotropic viscoelastic forces and generated active stresses. Active turbulence in nematic materials inevitably coexists with another intriguing phenomenon - continuous proliferation and annihilation of topological defects,[10–13] localized singularities of the order parameter, and is a subject of extensive study. With the notable exception of classical granular nematic systems comprised of vertically vibrated elongated particles (rods, ellipses, etc.) demonstrating nematic ordering, giant number fluctuations, and rich defect dynamics,[5,14–17] the vast majority of active nematic systems is of biological origin.[18,19] The leading example is a mixture of filamentary proteins and molecular motors that generate activity through adenosine triphosphate (ATP) hydrolysis converting chemical energy into a mechanical motion.[7,20] Another system, named Living Liquid Crystal (LLC), is a composite of a water-based liquid crystal and live swimming bacteria.[8,21] The hydrodynamic flows created by bacteria flagella exert local microscopic stress on the liquid crystal, causing disturbances in a long-range nematic order. The activity level in these two systems is controlled by the ATP and bacterial concentration, respectively. Both of these biological active nematic systems exhibit inherent variability due to differences in biological components and are subject to unavoidable biological aging (degradation). Moreover, biosynthetic systems have a very limited range of accessible activity levels.[22,23] By design, synthetic nematic systems are stable, provide access to a broader range of activity, and free from the deficiencies of the biologically-based ensembles. Nevertheless, classical granular nematic systems, while fully synthetic, lack the viscoelastic properties of biological nematics that significantly decrease the complexity of available dynamic phases.

Here, we report the realization of a fully synthetic active liquid crystalline system - acoustically energized liquid crystal (AELC) - free from biological agents or supplementary motile components, and with the activity level controlled externally in a wide range by the amplitude of the acoustic field. This active material does not just mimic certain liquid crystalline properties, it is an authentic liquid crystal with active extensile stress introduced by an acoustic field. In addition to exhibiting nematic ordering, this active liquid crystal demonstrates optical birefringence, anisotropic viscosity, and elasticity, undergoes phase transitions with temperature, a bi-phase state, and is tunable by electromagnetic fields. The system enables fast (with the response time

A. Sokolov, J. Katuri, J. J. de Pablo, A. Snezhko
Materials Science Division
Argonne National Laboratory
9700 South Cass Avenue, Lemont, IL 60439, USA
E-mail: sokolov@anl.gov
J. J. de Pablo
Pritzker School of Molecular Engineering
University of Chicago
Chicago, IL 60637, USA

The ORCID identification number(s) for the author(s) of this article can be found under https://doi.org/10.1002/adma.202418846

DOI: 10.1002/adma.202418846

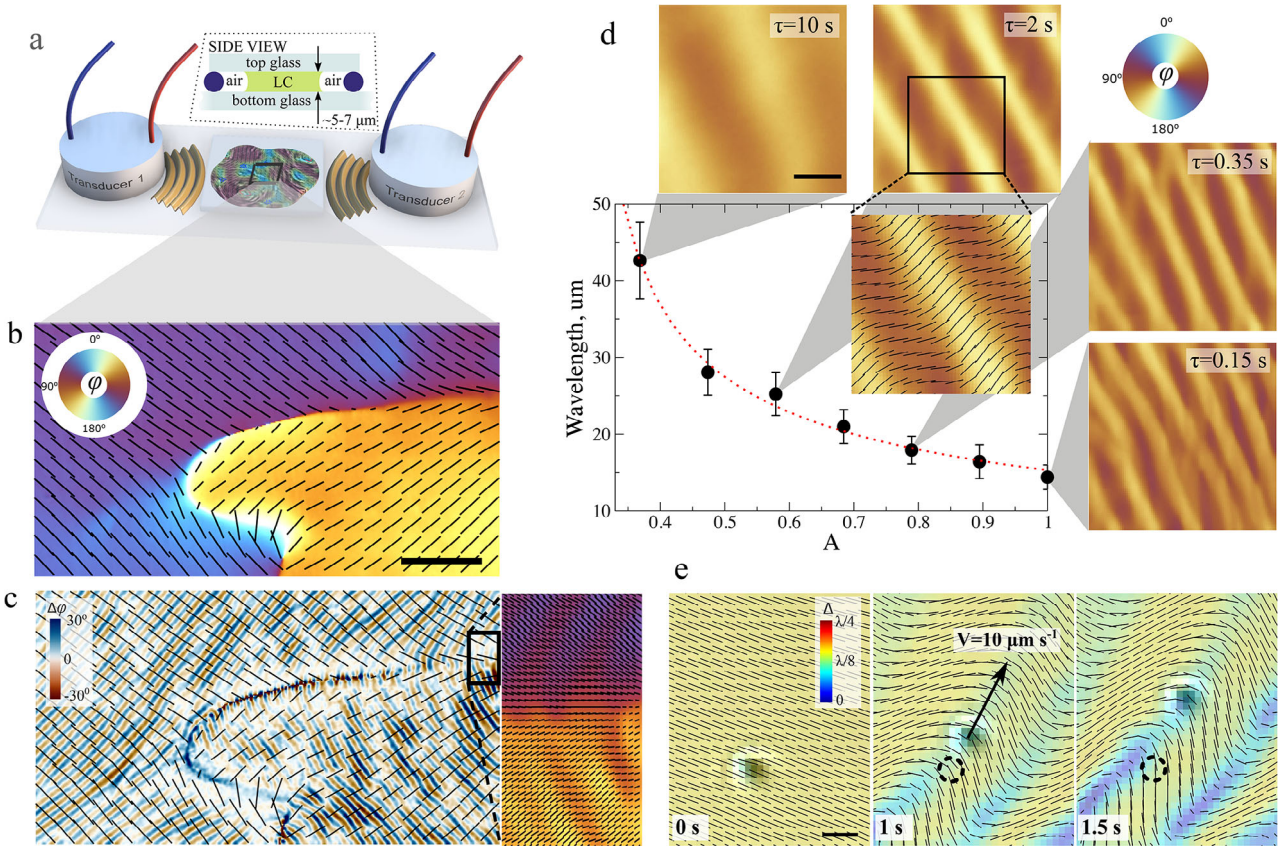

Figure 1. Acoustically energized liquid crystals. a) Schematic representation of the experimental setup. A droplet of DSCG is sandwiched between two glass slides and acoustically energized by two transducers attached to the bottom slide. b) An example of the spatial configuration of the director (black line segments) in two distinct domains before the ultrasound was applied. The color represents the local orientation angle φ according to the colormap in the top left corner. The scale bar is 50 μm. c) The deflection angle $\Delta\varphi$ of the local director upon application of the excitation signal. The stripes of the undulations are normal to the local orientation of the director. d) Dependence of the wavelength of the observed undulation on the amplitude of the acoustic field. The dot line shows the fit $\approx 1/\sqrt{A-a_0}$) where $a_0 = 0.27$. The inset images demonstrate patterns that emerged in DSCG at the corresponding amplitudes of the acoustic field. The scale bar is 20 μm. The error bars correspond to standard deviations of the mean values. e) Advection of a microscopic particle by the flow produced by undulation instability upon application of the acoustic field. The diameter of the particle is 3 μm. The color indicates the local optical retardance. The scale bar is 5 μm.

below 1ms) control of the activity (a typical microtubule/motor protein system has a response time from seconds to minutes), and a significantly extended range of the accessible activity levels compared to any biologically based active nematics. We experimentally demonstrate the conversion of the acoustic energy into local extensile stresses of the liquid crystalline media, resulting in the emergence of undulation instability with the characteristic wavelengths governed by the amplitude of the acoustic field. Acoustically energized liquid crystals bridge the gap between biologically based and synthetic granular nematics by accessing the viscoelastically governed, out-of-equilibrium behavior of biological active nematics at the microscale, while benefiting from controllability, repeatability, absence of degradation, and access to a significantly wider activity range of synthetic granular nematics. As the activity increases, the system transitions into a state characterized by a chaotic generation, motion, and annihilation of topological defects. We reveal the spontaneous formation of the unconventional free-standing persistent hydrodynamic vortices at high activity levels not previously observed in biologically-based active nematic systems.

2. Result and Discussion

The experimental system consists of the lyotropic chromonic (aqueous solution of self-assembled aromatic compounds) liquid crystals DSCG (disodium cromoglycate), sandwiched between two glass plates (6 μm sample thickness) with a pair of ultrasonic transducers glued to the bottom glass, see **Figure** 1a. DSCG is a water-based liquid crystal formed by the columnar aggregates of disk-like molecules with the diameter 1.6 nm and typical length 25–80 nm.[24] It was previously demonstrated that for the thin films with thickness less than 20 μm the orientation of the director remains in the plane of the experimental glass plates.[8,25] Consequently, it can be reconstructed from the birefringence map captured by a digital polarization camera using the 2D approximation. An example of a reconstructed director field is shown in Figure 1b, where two distinctive domains of the director field are observed. When the transducers are energized by a sinusoidal signal at ultrasonic frequencies (126 kHz for results shown in Figure 1c), the acoustic waves propagate through the glass and the LC medium, inducing reconfigurations in the

initially uniform director field in each domain, see also Movie S1 (Supporting Information). Within a fraction of a second, we observed the formation of a stripe pattern formed by periodic director undulations (Figure 1c, d), similar to those caused by local extensile stresses in other nematic active systems such as Living Liquid Crystal,[8] and mixtures of bio-filaments and molecular motors.[26–30]

The bending instability in active nematic systems is usually accompanied by induced hydrodynamic flows normal to the local orientation of the director field.[8,26,27] To confirm the presence of similar flows in our system, we added small tracers (2.2 μm in diameter) and tracked their motion upon application of the acoustic field, see Figure 1e and Movies S2 and S3 (Supporting Information). The direction of the tracers' motion matched the director field bending.

Experiments performed at various amplitudes and frequencies of the excitation signal reveal two key features of the observed bending instability: i) the orientation of the stripes is perpendicular to the initial local director field, as shown in Figure 1b, c, ii) the wavelength (λ) of the bending instability decreases with the amplitude of the applied voltage (A, normalized by maximum voltage of 20 V) as $\lambda \sim 1/\sqrt{A - a_0}$, where a_0 is a small constant (Figure 1d) corresponds to a minimum amplitude of the acoustic field resulting in the emergence of undulations in our experimental cell. The bending instability can be turned by adjusting the elasticity and viscosity of the liquid crystalline media. We observe the decrease of the wavelength λ with temperature due to reductions in both elasticity and viscosity of the media, see Figure S3 (Supporting Information) for details. Such response of the system qualitatively and quantitatively mimics the behavior of active nematic systems with extensile stress, such as Living Liquid Crystals or microtubules-molecular motors systems.[8,18,29,31]

Analogously to biological active nematic systems, the injection of activity in the liquid crystal by the acoustic field leads to the spontaneous topological defect proliferation causing the destruction of long-range nematic order and the emergence of an state characterized by a chaotic-like behavior of topological defects, see **Figure** 2a and Movie S4 (Supporting Information). The mechanism of bending instability is well-understood in biological active nematic systems and is the result of active extensile stress $\mathbf{\Sigma}^a = \alpha\mathbf{Q}$, where α is activity parameter ($\alpha < 0$ corresponds to an extensile stress) and $\mathbf{Q} = S(n_j n_j - \delta_{ij}/2)$ is an orientational tensor describing local alignment of liquid crystal molecules $\mathbf{n}$ and the local order parameter S.[29,32–34] In these systems the active stress $\mathbf{\Sigma}^a$ is generated by hydrodynamic flows created by swimming bacteria or forces exerted by molecular motors with the activity parameter α proportional to the magnitudes of these flows or forces. The observations of the acoustically powered LC system suggest that the ultrasonic wave in our experimental setup generates similar extensile microscopic stresses $\mathbf{\Sigma}^a$ that drive the liquid crystal out of equilibrium, and the absolute value of the activity parameter $|\alpha|$ increases linearly with the applied voltage to the ultrasonic transducer.

While the evidence of extensile active stresses in the AELC system is well-documented, the mechanisms responsible for the conversion of acoustic energy into a mechanical motion of the LC director field are not obvious. In general, ultrasound waves affect liquid crystals in various ways, such as inducing flow, altering the orientation of the liquid crystal molecules, and creating static patterns in the liquid crystal structure. For example, it was previously shown that the orientation of LC molecules can be changed statically and uniformly in space by acoustic radiation force.[35–39] Reorientation of LC molecules[40] and the emergence of periodic stripes and patterns were also attributed to acoustic streaming as a result of ultrasonic compression field.[41–43] In all these works, the period of the observed static patterns is defined either by the thickness of the experimental cell[41,42] or the excitation frequency.[43] In addition, the orientation of the observed stripes is parallel to LC/air interface. Periodical domain structures in LC (5CB) may also be induced by the elastic wave propagating in the glass plate.[44,45] However, the wavelength decreases with the excitation frequency (2–25 MHz range) and is observed either parallel or perpendicular to the acoustic wave direction. None of these previously reported phenomena apply to the reported here behavior.

In our system, we did not detect any averaged flows preceding the observed undulation instability. The stripes emerge always perpendicular to the local orientation of the director field (see Figure 1c), and what is more important, the period of the striped structure is controlled by the amplitude of the acoustic wave, not by the frequency or geometry of the experimental setup. In addition, only lyotropic chromonic liquids such as DSCG or Sunset Yellow showed the bending instability and other phenomena described below, while other liquid crystals like MBBA, 5CB, and 8CB did not exhibit these features. Both, DSCG and Sunset Yellow are comprised of rod-like aggregates of disk-shaped molecules (see Supporting Information and Figure S2, Supporting Information) in a liquid (water) and have a very strong anisotropy in viscosity and elasticity.[46] The rapid oscillatory compression of the LC droplet induces oscillatory flows predominantly along the local director field because of the much lower viscosity in this direction. These flows promote on-course collisions and sliding between rod-like aggregates of DSCG molecules resulting in the emergence of the extensile stresses in the system, the mechanism is similar to the one suggested for shaken granular rods nematic ensembles.[17,47,48]

As the level of activity increases with the amplitude of the acoustic wave, the undulations transition into the state of chaotic topological defects motion, see Figure 2a and Movie S4 (Supporting Information). In active nematic systems the turbulent state is often manifested by a chaotic reconfiguration of the director field and continuous proliferation/annihilation of topological defects.[7,11,49–52] The rich phenomenology of active turbulence comes from the complexity of active nematodynamics.[53–56] Because of the distinct geometrical structure of topological defects, the initial positive defects align parallel to the bending stripes and perpendicular to the original orientation of the director field, see Figure 2c. The positive defects start to move along the stripes while negative defects remain mostly stationary. Eventually, the system reaches a well-developed chaotic state, and the orientation of positive defects becomes isotropic, Figure 2a,c and independent of the initial orientation of the director field. Once the activity is removed, the chaotic defect motion state relaxes back to a uniformly aligned configuration. To quantify the evolution of the nematic order upon application of the acoustic field we calculate the angular speed $\Omega = \langle|\dot{\mathbf{n}}|\rangle$ and the curvature $K = \langle|(\mathbf{n} \cdot \nabla)\mathbf{n}|\rangle$ of the director field averaged over the observation area, as well as the density of topological defects N_D. A typical temporal

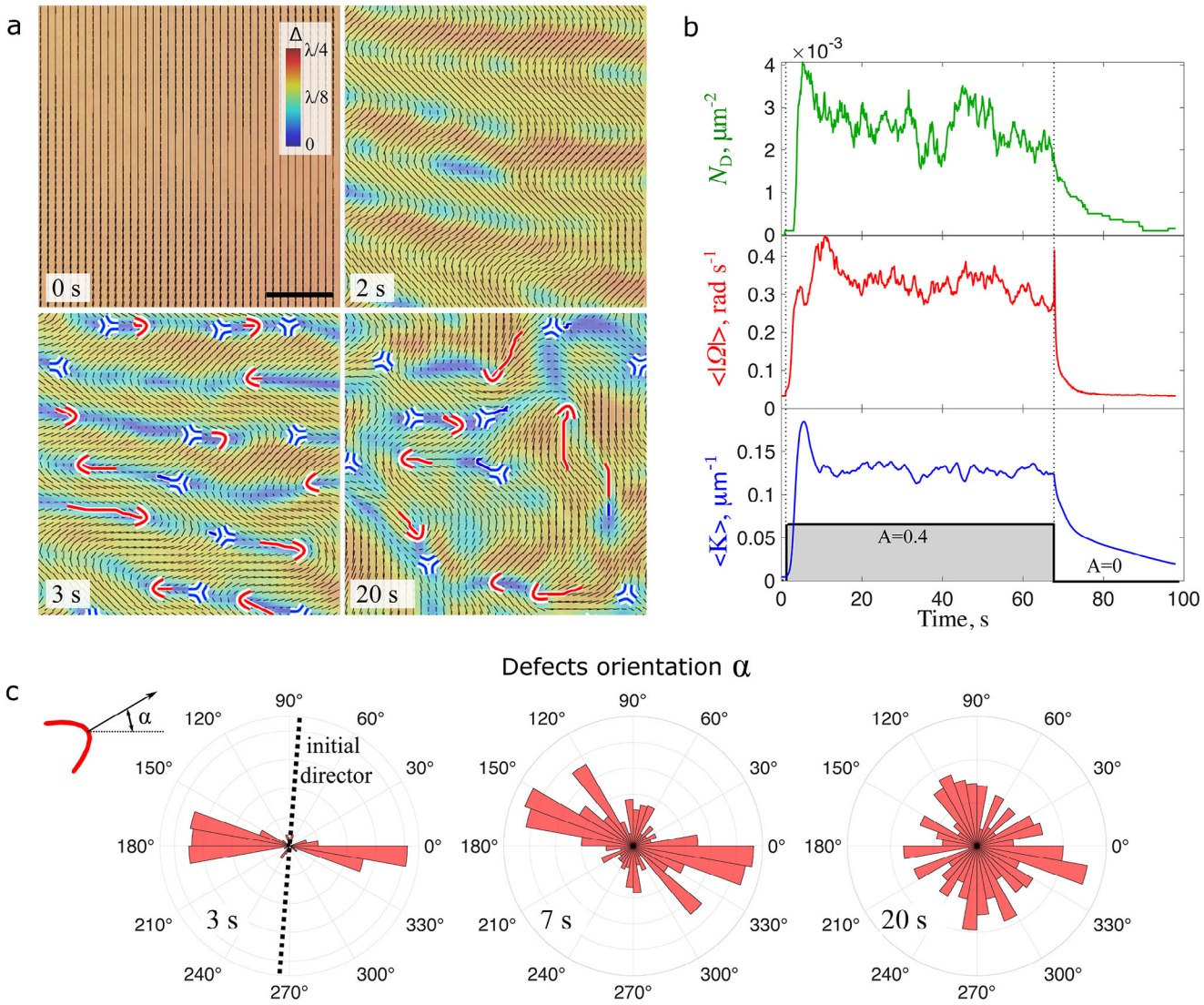

Figure 2. Proliferation of topological defects in acoustically powered liquid crystal. a) Reconstructed director fields (short black lines) and the optical retardance Δ (color) at different moments elapsed since the application of the acoustic field. The uniformity of the optical retardance field (shown in the top left corner) in the state preceding the application of the acoustic field, suggests the absence of local concentration variations across the sample. Topological defects are shown by red (+1/2 defect) and blue (-1/2 defect) symbols. The trajectories of positive and negative defects over one second are indicated by red and blue lines, respectively. The scale bar is 15 μm. b) Temporal evolution of the average director rotation rate $\langle|\Omega|\rangle$, curvature K and defects density N_D upon application of the acoustic field. The AELC is energized between 1 s and 68 s at the amplitude of $A = 0.4$. Non-zero Ω before and after the active period reflects the thermal fluctuations of liquid crystal molecules and camera noise. c) A polar histogram of positive topological defect orientations shown in (a) at different times (3, 7, and 20 s) elapsed since the application of the acoustic field. Initially, the defects are aligned with the emerging undulations resulting in anisotropic distribution of the defect orientations (left panel). The distribution becomes isotropic as the system evolves toward the regime of chaotic topological defects motion.

evolution of these parameters in AELC is shown in Figure 2b. The system reaches a steady dynamic state at the order of 10 s. Interestingly, Ω exhibits a distinct peak when the system is de-energized, which is also observed upon energizing the system. The spike is linked to a rapid relaxation of the elastic stresses in areas corresponding to a non-uniform structure of the director field (such as topological defects) upon removal of the external excitation. The director field undergoes a local rapid reconfiguration in the areas with the large elastic stress. Naturally, a strong spatial correlation between the local elastic energy and the speed of the director rotations is expected and observed, see **Figure** 3a,b.

The ability to control activity on demand allows us to probe the active states at a wide range of activity levels in a single experiment (often not achievable in bio-based systems). Characteristic reconfiguration speed of the director field Ω, the average curvature K, and the defects density N_D in a steady chaotic defects motion state as a function of the activity A are presented in Figure 3b,d. Assuming that hydrodynamic vorticity is linearly proportional to the rotational activity of the director field, the linear increase of Ω suggests a direct proportionality between the hydrodynamic vorticity and activity. Furthermore, the number of topological defects N_D demonstrates almost

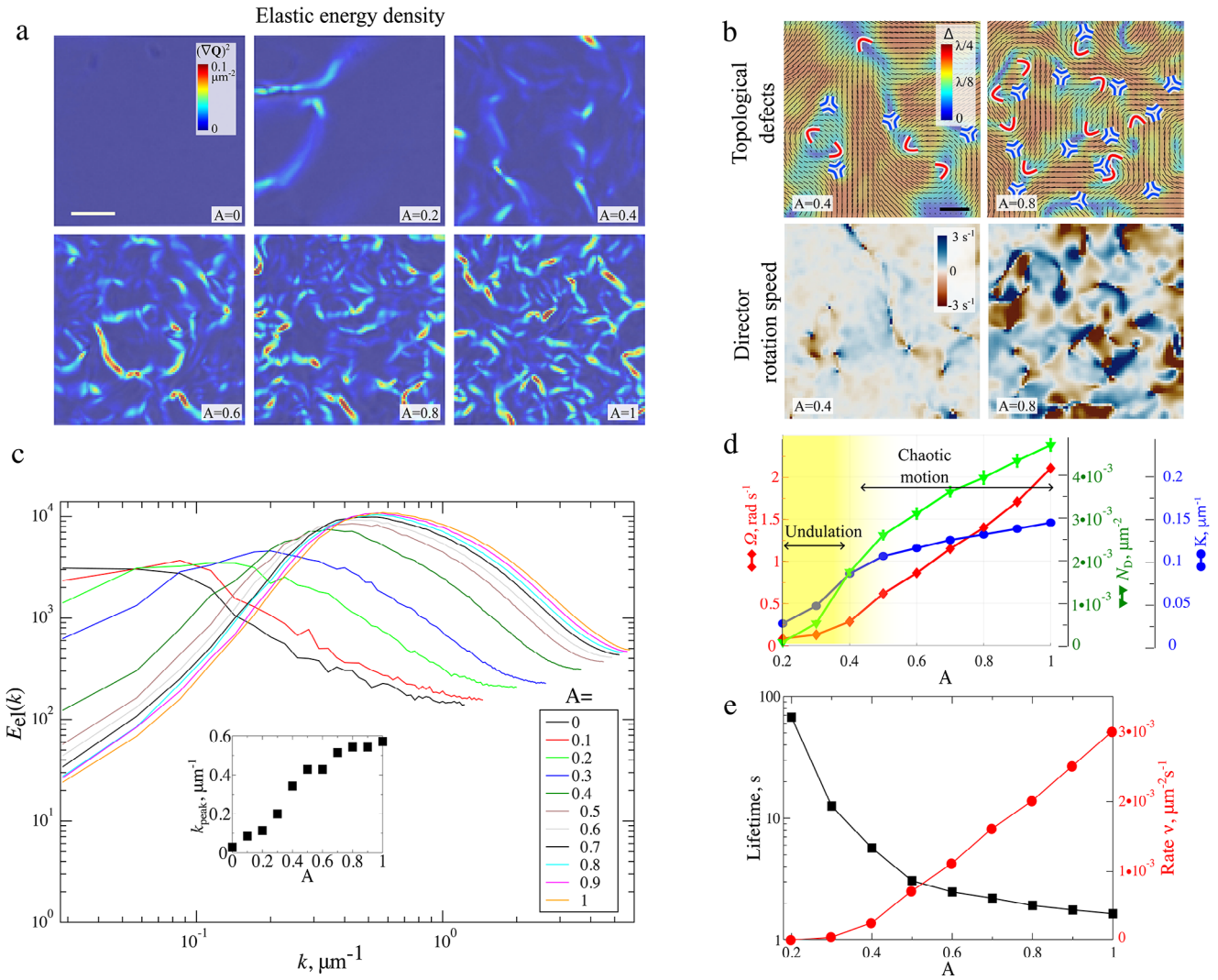

Figure 3. Spatiotemporal properties of acoustically energized liquid crystal in a state of a chaotic topological defects motion. a) Spatial distribution of the elastic energy density for various activity levels. b) Top: Director field (black lines) and phase retardance maps for A = 0.4 and A = 0.8. Bottom: Distribution of the local director rotational speed. c) Timed averaged elastic energy spectrum at different activity levels. Inset: Position of the elastic energy spectrum maximum as a function of activity. d) Dependence of the space- and time-averaged magnitude of the rotation speed Ω, the local curvature *K* of the director field, and the topological defects density N_D on the activity *A*. The undulation instability regime is highlighted in yellow for $A < 0.4$, while a chaotic defect motion is observed for $A > 0.4$. e) The average lifetime of defects (black squares) and the defect generation/annihilation rate (red circles) at different amplitudes of the acoustic field.The error bars (standard deviation of the mean) in panels (d) and (e) are comparable to or smaller than the size of a symbol.

linear increase with the activity, consistent with previous theoretical findings.[52,57] The defect generation rate ν increases with the activity, while the average lifetime of the defects decreases, see Figure 3e, due to an increase in the defect recombination probability.

We further investigated an elastic energy spectrum and its relationship to the activity by extracting the spatial distribution of elastic energy $(\nabla Q)^2$ in a 2D film of AELC, see Figure 3a. A typical spectrum has a peak that shifts towards smaller scales with the activity (see Figure 3c) in agreement with theoretical predictions for nematic systems.[58,59]

The velocity field in AELC in a well-developed regime of chaotic defects motion can be estimated by tracking the optical flow of birefringence patterns. The analysis of hydrodynamic vorticity in acoustically powered liquid crystal reveals an unexpected phenomenon - the emergence of disordered arrays of free-standing long-lived vortices at the high activity levels ($A > 0.5$), see **Figure** 4a,b, and Movies S5–S7 (Supporting Information). Ordered dynamic vortex patterns have been previously observed in simulations of confined extensible nematics[60–63] with vortex lattices accompanied by a dynamically ordered state of half-integer defects or novel states with vortices trapping pairs of +1/2 defects rotating coherently in the same direction while opposite vorticity was maintained by diffusive counter-rotating flows. Recently computational studies[64] have reported the emergence of ordered vortex lattices and coherent chiral motion of defect pairs in unconfined nematic fluids. In analogy with predictions[64] of the emergent vortical states observed in acoustically powered

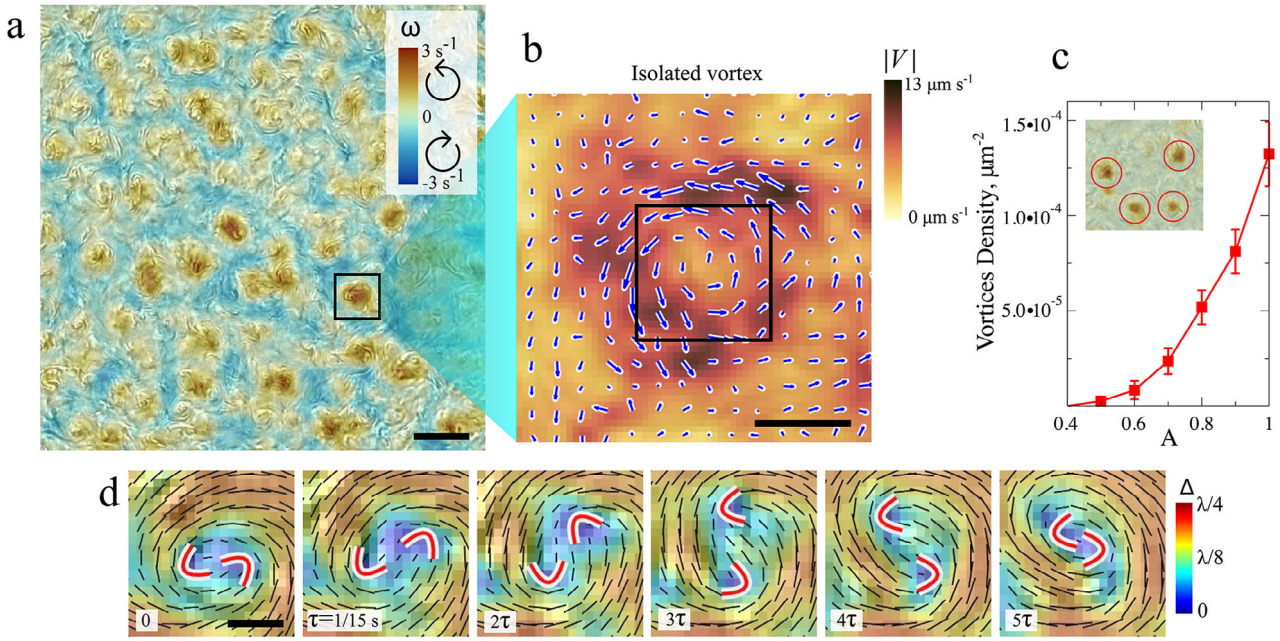

Figure 4. Free-standing vortices. a) A hydrodynamic vorticity map superimposed over the original raw image at $A = 0.8$. Brown and blue colors correspond to CCW and CW rotations respectively. The scale bar is 50 μm. See also Movie S5 (Supporting Information). b) The velocity field obtained by PIV in the vicinity of a single isolated vortex. The background color depicts the magnitude of the local velocity. The scale bar is 25 μm. c) The number of vortices in the field of view shown in (a) at different activity levels *A*. The vortices are identified by analyzing the Okubo-Weiss field and locating distinct regions where the field value falls below zero. The error bars correspond to standard deviations of the mean. d) Rotation of two positive defects in the core of the vortex. See also Movie S6 (Supporting Information). The scale bar is 5 μm.

liquid crystal are unconfined, with each vortex trapping a pair of +1/2 defects rotating with the same chiral state as the neighbors, see Figure 4a. In contrast to other experimental systems,[65,66] the vortices observed on our experiments are not ordered (see Figure S5 c,d, Supporting Information illustrating pair correlation functions and structure factors of the vortical ensemble). The vortices appear as localized round regions exhibiting high vorticity values. A typical vortex size is approximately 25 μm. A precise measurement of a vortex size is challenging due to the low resolution of the optical flow velocimetry method limited to 7 μm × 7 μm sub-window size. Strikingly, the majority of vortices within the same active domain exhibit consistent rotation in a single direction (clockwise or counterclockwise), nevertheless, the overall vorticity of a domain is zero. The zero net vorticity is maintained by counter-rotating flows in the interstitial region between the localized vortices. The polarity of vortices can alternate between different domains, see Movie S8 (Supporting Information). The direction of vortex rotation in domains can also be reversed by the acoustic field frequency (see Movie S9, Supporting Information). The intricate mechanism behind the spontaneous vortex generation, sorting into domains, and chirality control by the excitation frequency of the acoustic field is not clear at this point and represents an exciting challenge for future investigations. The vortex spatial density increases with the activity *A*, Figure 4c. The core of a typical vortex contains two circulating +1/2 defects (see Figure 4d; Movie S6, Supporting Information), resembling the observations in constrained active nematic systems.[67] In the unconstrained system, the circular motion of two positive defects around the center may be related to the bounding forces between active defects predicted theoretically.[68,69]

The use of acoustic fields enables unprecedented control over topological defect dynamics in active liquid crystal by the design of the microfluidic confinement or introduction of obstacles within the channel locally directing the flow of topological defects or efficiently injecting topological defects into the system (see Figure S4 and Movies S10 and S11, Supporting Information). The ability to inject, rectify, and direct the flows of topological defects in acoustically powered active liquid crystals is promising from the viewpoint of directed transport and logic operations with active topological defects in active nematics.[70] One of the potential limitations of the synthetic acoustically driven active liquid crystals is associated with unavoidable interactions of the acoustic waves with other materials (walls, cargo particle, etc) that may introduce undesirable noise, dynamics, and attenuation into the system. Also, while the biological active nematics units consume chemical fuels to generate activity at a local level, acoustically driven systems use external waves that may attenuate while propagating through the system, and multiple injection points may be required to address the acoustic signal attenuation in large systems.

3. Conclusion

In summary, we introduce a fully synthetic active liquid crystal comprised of a lyotropic chromonic liquid crystal (DSCG) energized by an ultrasound wave. The system is free from biological limitations (degradation, aging, actuation through consumption of a chemical fuel, limited range of activities) and demonstrates all phenomenology associated with active nematics - undulation instability, proliferation of topological defects, and their chaotic

motion. While the system reported here is quasi-2D by design, the physical mechanisms driving activity in acoustically powered liquid crystal can, in principle, be applicable to 3D geometries. Acoustically powered liquid crystals have stable physical properties and enable precise and rapid activity control over a significantly extended range. Access to significantly higher activity levels revealed the emergence of clusters of coherent nematic vortices. We demonstrate that the chaotic motion of topological defects in acoustically powered liquid crystal can be efficiently rectified by the design of the microfluidic channels or manipulated by the injection of topological defect flows by passive obstacles. The results provide a foundation for the unorthodox design of synthetic active nematic fluids with stable and tunable material properties.

4. Experimental Section

Sample Preparation and Experimental Details: The experimental system consisted of a small droplet (0.2 µL) of a lyotropic chromonic liquid crystal, disodium cromoglycate (DSCG, 13% by weight) water dispersion, confined between two glass slides and exposed to ultrasonic waves; see Figure 1a. Two ultrasonic transducers (H2KLPY11000600, DigiKey) were attached to the bottom slide and driven by a function generator (Agilent 33210a). The thickness of the LC droplets was controlled by spherical glass spacers and was approximately 4–5 µm. The experiments were conducted at a temperature of 20°C. In this experiments, the activity of LC depended on the frequency of the excitation signal with several strong response peaks specific to the geometry of a particular experimental cell. The data provided in this paper were collected for an excitation frequency of 126 kHz.

The phenomena presented in the paper were robust and had been reproduced across multiple realizations and trials. While the absolute magnitude of the measured quantities may vary between realizations due to factors such as varying acoustic field attenuation in different experimental cells, the reported trends remain consistent and reproducible.

The Reconstruction of the Director Field, the Optical Phase Retardance: A custom-built fast multi-polarization video-microscopy setup was used to detect and quantify the internal order of the active liquid crystal with high spatial and temporal resolution. The schematics of the developed optical system is shown in Figure S1a (Supporting Information), see also Ref. [71]. The LC film was illuminated with circularly polarized monochrome (590 nm) light. The camera sensor (Sony IMX250MZR), which consisted of a conventional light-sensitive sensor overlaid with an array of polarizers, captures four polarized images at different orientations 0^0, 45^0, 90^0, and 135^0 simultaneously. An example of a raw image is shown in Figure S1b (Supporting Information). Each 2×2 pixels block (highlighted by the red square for illustration) contained information about the direction and the degree of polarization. The liquid crystal in the nematic phase altered the polarization of light as a birefringent material. The local optical retardance in LC and the director field could be reconstructed from each 2x2 pixels block by using linear algebra (Jones calculus) and treating liquid crystal as a linear phase retarder. The schematic representation of such reconstruction is shown in Figure S1c,d (Supporting Information). If DSCG was illuminated by circularly polarized light and observed by the polarization camera, the brightness registered by each pixel can be expressed as

$$P_i = P_0\,(1 + \sin(\Gamma)\,\sin(2\alpha - 2\varphi_i)) \tag{1}$$

where $\Gamma = 2\pi\Delta n d/\lambda$ is the local optical retardance, α is the local orientation of the director field and φ_i is the orientation of the polarization filter of the i-th pixel. For the reconstruction of the director field and the order parameter the relative variations of intensities were first computed $\widetilde{P_i} = P_i/P_0 - 1$, where P_i is the pixel brightness in the same pixel block (see Figure S1b,c, Supporting Information), $P_0 = 1/4 \sum_{i=1..4} P_i$ is the average brightness used for the binned image, Figure S1e (Supporting Information). The local optical retardance Γ (proportional to the local order parameter) is calculated as:

$$\Gamma = \arcsin\left(\sqrt{\widetilde{P_1}^2 + \widetilde{P_2}^2}\right) \tag{2}$$

The local angle of the director field φ can be computed as:

$$\varphi = \frac{1}{2}\,\mathrm{sign}\left(\widetilde{P_1}\right)\arccos\frac{\widetilde{P_2}}{\sqrt{\widetilde{P_1}^2 + \widetilde{P_2}^2}} \tag{3}$$

To improve the accuracy of the noisy experimental data processing, a spatial Gaussian filter was applied. However, the director field cannot be oriented around topological defects to make it a continuous vector field. To resolve that issue, a vector field was introduced, produced by a doubled orientation angle φ with the amplitude proportional to the local order parameter. That additionally introduced vector field could be oriented even in the presence of topological defects and, correspondingly, be spatially filtered. The smoothed local director field was produced by reversing the procedure, or as halved of the angle of the filtered vector field. For the data presented in the main text the Gaussian filter with the $\sigma = 2$ pixels, which corresponds to ≈ 0.9 µm, was applied. The method of reconstruction of the director field by measuring the optical retardance imposes a constrain on maximum thickness d of the experimental cell. For a typical optical birefringence $\Delta n \approx -0.02$ for wt 14% DSCG,[72] increasing d beyond 8 µm introduces uncertainty attributed to the periodic nature of sin (Γ) function in Equation (1). This uncertainty could be overcome by scanning the liquid crystal with several different wavelengths and conducting a more complex analysis of the data.

Supporting Information

Supporting Information is available from the Wiley Online Library or from the author.

Acknowledgements

The research was supported by the U.S. Department of Energy, Office of Science, Basic Energy Sciences, Materials Sciences, and Engineering Division.

Conflict of Interest

The authors declare no conflict of interest.

Data Availability Statement

The data that support the findings of this study are available from the corresponding author upon reasonable request.

Keywords

active matter, active nematic, liquid crystals, topological defects

Received: December 2, 2024
Revised: March 10, 2025
Published online: March 26, 2025

[1] C. Dombrowski, L. Cisneros, S. Chatkaew, R. E. Goldstein, J. O. Kessler, *Phys. Rev. Lett.* **2004**, *93*, 098103.
[2] A. Doostmohammadi, S. P. Thampi, J. M. Yeomans, *Phys. Rev. Lett.* **2016**, *117*, 048102.
[3] G. Duclos, C. Erlenkämper, J.-F. Joanny, P. Silberzan, *Nat. Phys.* **2017**, *13*, 58.
[4] R. Mueller, J. M. Yeomans, A. Doostmohammadi, *Phys. Rev. Lett.* **2019**, *122*, 048004.
[5] V. Narayan, S. Ramaswamy, N. Menon, *Science* **2007**, *317*, 105.
[6] I. Vélez-Cerón, P. Guillamat, F. Sagués, J. Ignés-Mullol, *Proc. Natl. Acad. Sci.* **2024**, *121*, e2312494121.
[7] T. Sanchez, D. T. Chen, S. J. DeCamp, M. Heymann, Z. Dogic, *Nature* **2012**, *491*, 431.
[8] S. Zhou, A. Sokolov, O. D. Lavrentovich, I. S. Aranson, *Proc. Natl. Acad. Sci.* **2014**, *111*, 1265.
[9] S. Shankar, L. V. Scharrer, M. J. Bowick, M. C. Marchetti, *Proc. Natl. Acad. Sci.* **2024**, *121*, e2400933121.
[10] S. P. Thampi, R. Golestanian, J. M. Yeomans, *EPL (Europhysics Letters)* **2014**, *105*, 18001.
[11] L. Giomi, M. J. Bowick, P. Mishra, R. Sknepnek, M. Cristina Marchetti, *Phil. Trans. R. Soc. A.: Math., Phys. Eng. Sci.* **2014**, *372*, 20130365.
[12] N. Kumar, R. Zhang, S. A. Redford, J. J. de Pablo, M. L. Gardel, *arXiv preprint arXiv:2204.00113* **2022**.
[13] L. C. Head, C. Doré, R. R. Keogh, L. Bonn, G. Negro, D. Marenduzzo, A. Doostmohammadi, K. Thijssen, T. López-León, T. N. Shendruk, *Nat. Phys.* **2024**, *20*, 492.
[14] V. Narayan, N. Menon, S. Ramaswamy, *J. Stat. Mech.: Theory Exp.* **2006**, *2006*, P01005.
[15] A. Kudrolli, G. Lumay, D. Volfson, L. S. Tsimring, *Phys. Rev. Lett.* **2008**, *100*, 058001.
[16] P. Arora, A. Sood, R. Ganapathy, *Phys. Rev. Lett.* **2022**, *128*, 178002.
[17] H. Soni, N. Kumar, J. Nambisan, R. K. Gupta, A. Sood, S. Ramaswamy, *Soft Matter* **2020**, *16*, 7210.
[18] A. Doostmohammadi, J. Ignés-Mullol, J. M. Yeomans, F. Sagués, *Nat. Commun.* **2018**, *9*, 1.
[19] R. Zhang, A. Mozaffari, J. J. de Pablo, *Nat. Rev. Mater.* **2021**, *6*, 437.
[20] F. Ndlec, T. Surrey, A. C. Maggs, S. Leibler, *Nature* **1997**, *389*, 305.
[21] A. Sokolov, A. Mozaffari, R. Zhang, J. J. De Pablo, A. Snezhko, *Phys. Rev. X* **2019**, *9*, 031014.
[22] R. Zhang, S. A. Redford, P. V. Ruijgrok, N. Kumar, A. Mozaffari, S. Zemsky, A. R. Dinner, V. Vitelli, Z. Bryant, M. L. Gardel, et al., *Nat. Mater.* **2021**, *20*, 875.
[23] P. V. Ruijgrok, R. P. Ghosh, S. Zemsky, M. Nakamura, R. Gong, L. Ning, R. Chen, V. T. Vachharajani, A. E. Chu, N. Anand, et al., *Nat. Chem. Biol.* **2021**, *17*, 540.
[24] H. Baza, T. Turiv, B.-X. Li, R. Li, B. M. Yavitt, M. Fukuto, O. D. Lavrentovich, *Soft Matter* **2020**, *16*, 8565.
[25] H.-S. Park, O. D. Lavrentovich, *Liq. Cryst. Beyond Displ.: Chem., Phys., Appl.* **2012**, *14*, 449.
[26] T. Gao, R. Blackwell, M. A. Glaser, M. D. Betterton, M. J. Shelley, *Phys. Rev. Lett.* **2015**, *114*, 048101.
[27] B. Martínez-Prat, J. Ignés-Mullol, J. Casademunt, F. Sagués, *Nat. Phys.* **2019**, *15*, 362.
[28] A. Senoussi, S. Kashida, R. Voituriez, J.-C. Galas, A. Maitra, A. Estevez-Torres, *Proc. Natl. Acad. Sci.* **2019**, *116*, 22464.
[29] R. A. Simha, S. Ramaswamy, *Phys. Rev. Lett.* **2002**, *89*, 058101.
[30] R. Voituriez, J.-F. Joanny, J. Prost, *EPL (Europhysics Letters)* **2005**, *70*, 404.
[31] S. Ramaswamy, M. Rao, *New J. Phys.* **2007**, *9*, 423.
[32] S. Thampi, J. Yeomans, *Eur. Phys. J. Spec. Top.* **2016**, *225*, 651.
[33] E. J. Hemingway, P. Mishra, M. C. Marchetti, S. M. Fielding, *Soft Matter* **2016**, *12*, 7943.
[34] P. Srivastava, P. Mishra, M. C. Marchetti, *Soft matter* **2016**, *12*, 8214.
[35] D. Koyama, R. Isago, K. Nakamura, *Appl. Phys. Lett.* **2012**, *100*, 091102.
[36] Y. Shimizu, D. Koyama, M. Fukui, A. Emoto, K. Nakamura, M. Matsukawa, *Appl. Phys. Lett.* **2018**, *112*, 161104.
[37] Y. J. Liu, M. Lu, X. Ding, E. S. Leong, S.-C. S. Lin, J. Shi, J. H. Teng, L. Wang, T. J. Bunning, T. J. Huang, *J. Lab. Autom.* **2013**, *18*, 291.
[38] J. Selinger, M. Spector, V. Greanya, B. Weslowski, D. Shenoy, R. Shashidhar, *Phys. Rev. E* **2002**, *66*, 051708.
[39] M. Witkowska-Borysewicz, A. Sliwiński, *J. Phys.* **1983**, *44*, 411.
[40] R. Ozaki, T. Shinpo, M. Ozaki, H. Moritake, *Jpn. J. Appl. Phys.* **2007**, *46*, L489.
[41] O. Kapustina, *Crystallogr. Rep.* **2004**, *49*, 680.
[42] O. Kapustina, *Acoust. Phys.* **2008**, *54*, 180.
[43] C. Sripaipan, C. F. Hayes, G. T. Fang, *Phys. Rev. A* **1977**, *15*, 1297.
[44] H. M. H. Moritake, T. S. T. Seike, K. T. K. Toda, *Jpn. J. Appl. Phys.* **1999**, *38*, 3076.
[45] R. Ozaki, M. Aoki, H. Moritake, K. Yoshino, K. Toda, *Jpn. J. Appl. Phys.* **2006**, *45*, 4662.
[46] S. Zhou, in *Lyotropic Chromonic Liquid Crystals: From Viscoelastic Properties to Living Liquid Crystals*, Springer, Berlin **2017**, pp. 51–75.
[47] L. Bonn, A. Ardaševa, R. Mueller, T. N. Shendruk, A. Doostmohammadi, *Phys. Rev. E* **2022**, *106*, 044706.
[48] F. Vafa, M. J. Bowick, B. I. Shraiman, M. C. Marchetti, *Soft Matter* **2021**, *17*, 3068.
[49] V. Schaller, A. R. Bausch, *Proc. Natl. Acad. Sci.* **2013**, *110*, 4488.
[50] F. C. Keber, E. Loiseau, T. Sanchez, S. J. DeCamp, L. Giomi, M. J. Bowick, M. C. Marchetti, Z. Dogic, A. R. Bausch, *Science* **2014**, *345*, 1135.
[51] M. J. Bowick, N. Fakhri, M. C. Marchetti, S. Ramaswamy, *Phys. Rev. X* **2022**, *12*, 010501.
[52] L. Giomi, *Phys. Rev. X* **2015**, *5*, 031003.
[53] P.-G. De Gennes, J. Prost, *The physics of liquid crystals*, vol. *83*, Oxford university press, Oxford **1993**.
[54] C. Peng, T. Turiv, Y. Guo, Q.-H. Wei, O. D. Lavrentovich, *Science* **2016**, *354*, 882.
[55] P. C. Mushenheim, R. R. Trivedi, H. H. Tuson, D. B. Weibel, N. L. Abbott, *Soft Matter* **2014**, *10*, 88.
[56] N. D. Bade, R. D. Kamien, R. K. Assoian, K. J. Stebe, *Soft Matter* **2018**, *14*, 6867.
[57] S. Shankar, M. C. Marchetti, *Phys. Rev. X* **2019**, *9*, 041047.
[58] Ž. Krajnik, Ž. Kos, M. Ravnik, *Soft Matter* **2020**, *16*, 9059.
[59] C. Rorai, F. Toschi, I. Pagonabarraga, *Phys. Rev. Lett.* **2022**, *129*, 218001.
[60] A. Doostmohammadi, M. F. Adamer, S. P. Thampi, J. M. Yeomans, *Nat. Commun.* **2016**, *7*, 10557.
[61] T. N. Shendruk, A. Doostmohammadi, K. Thijssen, J. M. Yeomans, *Soft Matter* **2017**, *13*, 3853.
[62] S. Chandragiri, A. Doostmohammadi, J. M. Yeomans, S. P. Thampi, *Phys. Rev. Lett.* **2020**, *125*, 148002.
[63] C. D. Schimming, C. Reichhardt, C. Reichhardt, *Phys. Rev. Lett.* **2024**, *132*, 018301.
[64] F. Caballero, Z. You, M. C. Marchetti, *Soft Matter* **2023**, *19*, 7828.
[65] Y. Sumino, K. H. Nagai, Y. Shitaka, D. Tanaka, K. Yoshikawa, H. Chaté, K. Oiwa, *Nature* **2012**, *483*, 448.
[66] H. Xu, Y. Wu, *Nature* **2024**, *627*, 553.
[67] A. Opathalage, M. M. Norton, M. P. Juniper, B. Langeslay, S. A. Aghvami, S. Fraden, Z. Dogic, *Proc. Natl. Acad. Sci.* **2019**, *116*, 4788.
[68] S. Shankar, S. Ramaswamy, M. C. Marchetti, M. J. Bowick, *Phys. Rev. Lett.* **2018**, *121*, 108002.
[69] K. Thijssen, A. Doostmohammadi, *Phys. Rev. Res.* **2020**, *2*, 042008.
[70] R. Zhang, A. Mozaffari, J. J. de Pablo, *Sci. Adv.* **2022**, *8*, eabg9060.
[71] J. Katuri, A. Snezhko, A. Sokolov, *Soft Matter* **2022**, *18*, 8641.
[72] Y. A. Nastishin, H. Liu, T. Schneider, V. Nazarenko, R. Vasyuta, S. Shiyanovskii, O. Lavrentovich, *Phys. Rev. E* **2005**, *72*, 041711.